

Competing quantum effects in spin crossover chains: spin-orbit coupling, magnetic exchange, and elastic interactions

F. Rist,¹ H. L. Nourse,^{2,*} and B. J. Powell¹

¹*School of Mathematics and Physics, The University of Queensland, 4072, Australia*

²*Quantum Information Science and Technology Unit, Okinawa Institute of Science and Technology Graduate University, Onna-son, Okinawa 904-0495, Japan*

(Dated: August 23, 2024)

We derive and study a model of square planar, d^8 spin crossover materials that treats elastic, magnetic and spin-orbit interactions on an equal footing. For 1D chains density matrix renormalization group calculations show that the competition between these interactions leads to six different phases. For weak spin-orbit coupling (SOC) and large antiferromagnetic interactions we find a symmetry protected topological (SPT) Haldane phase. Moderate SOC introduces dynamical low-spin (LS) impurities that rapidly destroy the SPT state and drive the system into a topologically trivial high spin (THS) phase. This is equivalent to the Haldane–large-D phase transition driven by single ion anisotropy (D) in the spin-one Heisenberg model. For strong SOC the $S^z = \pm 1$ HS states are high-energy excitations. Thus, the system can be understood as a transverse field Ising model with the SOC playing the role of the transverse field. Consistent with this, we find a quantum phase transition between the THS phase and a quantum disordered (QD) phase. However, if the magnetic coupling is non-zero or the HS and LS states of a single molecule are non-degenerate the Z_2 (Ising) symmetry is broken and the phase transition becomes a crossover. Thus, the QD phase and the THS phases are adiabatically connected, as, equivalently, are the large-D phase of the spin-one Heisenberg model and the quantum disordered phase of the transverse field Ising model. We also find a ferroelastic LS phase, an antiferroelastic phase, with alternating HS and LS complexes, and a dimer phase, which results from the competition between antiferromagnetic and antiferroelastic interactions.

I. INTRODUCTION

Spin crossover (SC) materials hold enormous promise for applications in spintronics and molecular switches [1]. A SC molecule is a metal-organic complex with two stable spin states. This occurs due to the competition between ligand field splitting, which favors a low-spin (LS) state, and Coulomb repulsion (Hund’s rule coupling), which favors a high-spin (HS) [2]. Although SC is a property of the molecule, collective spin-state switching phenomena, such as multistep transitions [3–40], collective switching [41], light-induced spin-state trapping [42], thermal hysteresis [43], and complex relaxation of excited states [44–57] have been widely observed in SC collections. More exotic phases, including Devil’s staircases [58], dimer phases [59], spin-state semitics [60], spin-state ices [61], and other Coulomb phases [62], have been proposed.

The most widely discussed cause of these collective phenomena in SC materials is the elastic interactions between molecules, which couple the spin-states of molecules due to the large ($\sim 10\%$) change in metal-ligand bond lengths that accompany spin-state switching [63–66]. Elastic coupling can be either antiferroelastic or ferroelastic, i.e., can either favor neighbors with different spin states or the same spin states, respectively [61, 63]. Such interactions can give rise to long-ranged ordering of spin states [3–41]. Classical models, including Ising-like

and elastic models [61, 63–71], have been widely invoked to explained this plethora of experimentally observed SC phenomena.

However, SC materials can have important quantum effects arising from both magnetic exchange interactions [72] and spin-orbit coupling (SOC) [45, 71, 73, 74]. For example, density functional theory calculations show that Fe(II) triazole SC chains have magnetic spin exchange strengths of the same order as elastic coupling [72], yet these interactions are often either neglected or only included classically [64, 66, 68, 69, 75]. SOC is vital for SC as it allows (otherwise spin-forbidden) transitions between spin-states [45, 73].

Timm and Schollwöck [59] have previously studied the interplay between SC and antiferromagnetic exchange in one-dimensional chains of d^6 complexes, which have spin-zero LS states and spin-two HS states. For strong enough antiferromagnetic interactions they found that the ground state is in the (topologically trivial) $S = 2$ Haldane phase [76]. SC enriches the possible ground states by introducing spin-0 dynamical impurities which favor a long-ranged ordered dimer phase that is a compromise between magnetic and spin-state ordering.

However, Timm and Schollwöck did not investigate the effects of SOC in SC chains [59]. This means that, in their model, the spin-state (i.e., the total spin) of a complex is a constant of motion. Once SOC is included, this is not the case. We will show below that this has important consequences for the quantum many-body physics of SC chains.

SOC is well known to be important to spin crossover

* Present address: School of Chemistry, University of Sydney, NSW 2006, Australia

with its effects well studied [45, 71, 73, 74]. However, most work to date has focused on the effects of SOC in single SC molecules rather than its impact on collective effects. D’Avino *et al.* [74] carried out a detailed study of a phenomenological model of SOC in SC individual molecules. They also considered collective effects within the mean field approximation, noting that the SOC induces an effective transverse field in the Ising-like models of SC. However, they concluded that SOC only has “minor effects on the thermodynamic properties and transition curves” of SC materials. We will show below that this is not always the case. Nadeem *et al.* [45, 71] included SOC in a many-body theory of SC based on crystal field theory, but integrated out quantum effects and limited their discussion to a semi-classical theory.

Recently, Liu *et al.* [41] observed an antiferroelastic phase has been observed in chains of the nickel tetrahydrobenzene (NiTHB) on Au(111). This contrasts with most other SC chains, such Fe(II) 1,2,4-triazole, which show ferroelastic order. Density functional calculations suggest that the strain due to binding to the substrate may be important in stabilising the antiferroelastic phase at low temperatures. Consistent with this, at low temperatures NiTHB is in the LS phase on Au(100), where the Ni-Ni distance is smaller than on Au(111), and the HS phase on Au(110), where the Ni-Ni distance is larger than on Au(111) [77]. Liu *et al.* also demonstrated dynamical collective spin-state switching between the HLHLHL... and LHLHLH... states, suggesting that such phases could be useful for data storage. While we will not attempt to model NiTHB specifically, this motivates us to study square planar SC complexes, which are highly compatible with growth on a surface. The d^8 filling, relevant to NiTHB, is also particularly interesting as SOC allows transitions between the ($S = 1$) HS and ($S = 0$) LS states at first order (in the SOC strength). This contrasts with the common example of Fe(II), which is d^6 , where the ($S = 2$) HS and ($S = 0$) LS states are only coupled at second order via an ($S = 1$) intermediate spin state [45, 73]. This suggests that the effects of SOC may be more prominent d^8 complexes.

This Article is organised as follows. In Section II we derive an effective low-energy model of SC in d^8 square planar spin crossover complexes. This model treats elastic interactions, SOC, and magnetic exchange on an equal footing. We show that SOC gives rise to a term that behaves as a single ion anisotropy for the physical spin and a transverse field for the pseudo-spins that label the spin-states of the molecules. In Section III we describe our density matrix renormalisation group (DMRG) calculations for this model. In Section IV we report the results of these calculations. They reveal a complicated zero temperature phase diagram containing six phases. We find that (anti)ferroelastic interactions favor (anti)ferroelastic spin-state order [specifically, the LS, Fig. 1a, trivial HS (THS) Fig. 1b; and antiferroelastic (AFE), Fig. 1c, phases]. Exchange interactions favor a symmetry protected topological (SPT) Haldane high spin

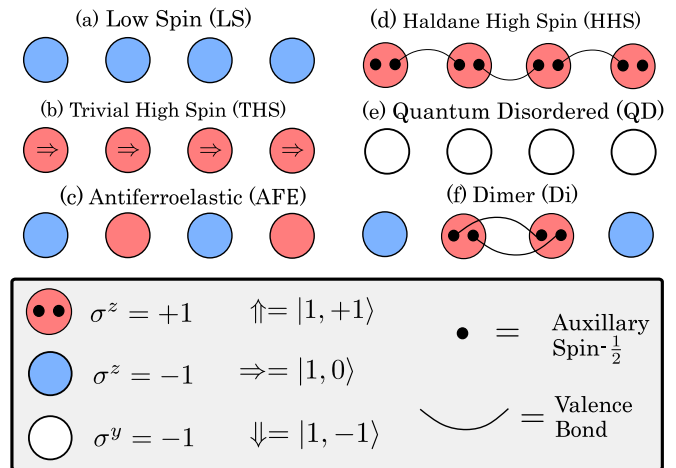


FIG. 1. Schematic of the groundstates found in our simple model of square planar, d^8 , spin crossover complexes with magnetic exchange and spin-orbit coupling [Eq. (9)]. The colour of a site represents the spin-state (pseudo-spin), with red corresponding to spin-one, high-spin (HS; $\sigma^z = 1$), blue to spin-zero, low-spin (LS; $\sigma^z = -1$), and white to a superposition of HS and LS ($\sigma^y = -1$). Arrows represent the S^z -projection of the spin. In the dimer and Haldane phases each spin-one can be represented by two spin-1/2s, which form spin-singlets (valence bonds) with the spin-1/2s on neighboring sites.

(HHS) phase (Fig. 1d) [78–82]) SOC favors a quantum disordered (QD) phase (Fig. 1e), similar to that found in the high-field limit of the transverse Ising model [83]). There is strong competition between these interactions leading to a complex phase diagram, that also contains a dimer phase (Fig. 1f), similar to that discovered by Timm and Schollwöck [59], which is compromise between the antiferroelastic and antiferromagnetic interactions.

II. MODEL

A. Low-energy subspace of a SC complex

Square planar complexes typically have a large splitting between the t_{2g} and e_g orbitals of the metal ions. Thus, for d^8 complexes the t_{2g} orbitals will be fully occupied and we need consider only the e_g orbitals, Fig. 2. The Aufbau principle predicts a LS singlet state with both electrons in the d_{xy} orbital, whereas Hund’s first rule predicts a HS triplet with one electron in each of d_{xy} and $d_{x^2-y^2}$ orbitals. Thus, these are the electronic configurations one expects to be energetically competitive in a square planar d^8 complex [84].

The simplest possible model therefore consists of a low-energy subspace in which each complex can take only these four possible states (i.e., the LS or one of the three HS states). We denote the electronic state of the i th ion $|\sigma^z, S^z\rangle_i$, where the pseudo-spin $\sigma^z = -1$ (+1) indicates that the ion is LS (HS) and S^z is the projection of the

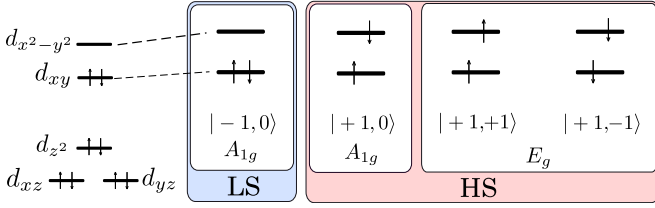


FIG. 2. The orbital structure of a d^8 square planar spin crossover (SC) complex. The low-energy subspace consists of the LS (a singlet, with both electrons in the d_{xy} orbital) and the HS (a triplet, with one electron in the d_{xy} orbital and another in the $d_{x^2-y^2}$ orbital). We denote these four spin states $|\sigma^z, S^z\rangle$, where σ^z is the z projection of a pseudospin that labels the spin-state ($\sigma^z = -1$ for LS and $\sigma^z = 1$ for HS) and S^z is the z projection of the physical spin. A_{1g} and E_g label the relevant irreducible representations of the D_{4h} double group.

metal ion's spin onto the z -axis. That is,

$$\begin{aligned}
 |-1, 0\rangle_i &= \hat{c}_{i,xy,\uparrow}^\dagger \hat{c}_{i,xy,\downarrow}^\dagger |0\rangle, \\
 |1, 0\rangle_i &= \frac{1}{\sqrt{2}} (\hat{c}_{i,xy,\uparrow}^\dagger \hat{c}_{i,x^2-y^2,\downarrow}^\dagger + \hat{c}_{i,xy,\downarrow}^\dagger \hat{c}_{i,x^2-y^2,\uparrow}^\dagger) |0\rangle, \\
 |1, 1\rangle_i &= \hat{c}_{i,xy,\uparrow}^\dagger \hat{c}_{i,x^2-y^2,\uparrow}^\dagger |0\rangle, \\
 |1, -1\rangle_i &= \hat{c}_{i,xy,\downarrow}^\dagger \hat{c}_{i,x^2-y^2,\downarrow}^\dagger |0\rangle,
 \end{aligned} \quad (1)$$

where $\hat{c}_{i,\nu,s}^\dagger$ creates an electron with spin s in the d_ν orbital of the i th ion, and $|0\rangle$ is the vacuum of the low-energy subspace.

The creation operators for the e_g -orbitals can be rewritten as [85]

$$\begin{aligned}
 \hat{c}_{i,x^2-y^2,s}^\dagger &= \frac{1}{\sqrt{2}} (\hat{a}_{i,2,s}^\dagger + \hat{a}_{i,-2,s}^\dagger), \\
 \hat{c}_{i,xy,s}^\dagger &= -\frac{i}{\sqrt{2}} (\hat{a}_{i,2,s}^\dagger - \hat{a}_{i,-2,s}^\dagger),
 \end{aligned} \quad (2)$$

where $\hat{a}_{i,l_m,s}^{(\dagger)}$ annihilates (creates) an electron on the i th ion with angular momentum l_m and spin s .

B. Wajnflasz–Pick–Ising model of spin crossover

We model collective SC effects via the Ising-like model for pseudo-spins introduced by Wajnflasz and Pick [65, 67]. The elastic interactions are described via a phenomenological parameter, J_I . We will describe the coupling as (anti)ferroelastic for ($J_I > 0$) $J_I < 0$. In general the different spin-states of an isolated SC complex will have different free-energies. This can be re-summed and included in the many-body Hamiltonian, whence the free-energy difference between HS and LS, ΔG , appears as an effective longitudinal field in the Ising-like model. For a chain of N complexes the model is

$$\hat{H}_{\text{WPI}} = J_I \sum_{j=1}^N \sigma_j^z \sigma_{j+1}^z + \Delta G \sum_{j=1}^N \sigma_j^z. \quad (3)$$

C. Magnetic exchange

Magnetic coupling between nearest neighbor metallic ions is facilitated by superexchange, mediated through the ligands:

$$\hat{H}_X = J_H \sum_{j=1}^N \hat{\mathbf{S}}_j \cdot \hat{\mathbf{S}}_{j+1}, \quad (4)$$

where $\hat{\mathbf{S}}_i = (\hat{S}_i^x, \hat{S}_i^y, \hat{S}_i^z)$ is the spin operator for the i th complex. We only consider antiferromagnetic coupling ($J_H > 0$) in accordance with the Goodenough-Kanamori rules [86]. This expectation has been confirmed by first principles calculations for SC compounds [72, 87], which also suggest that magnetic interactions are non-negligible in these materials.

D. Spin-orbit coupling

Spin-orbit coupling allows for inter-system crossing between electronic states, facilitating spin-state switching [45, 73]. This is given by

$$\hat{H}_{\text{SOC}} = \xi \sum_{j=1}^N \hat{\mathbf{L}}_j \cdot \hat{\mathbf{S}}_j, \quad (5)$$

where $\hat{\mathbf{L}}_i = (\hat{L}_i^x, \hat{L}_i^y, \hat{L}_i^z)$ is the orbital angular momentum operator on the i th complex and ξ is the spin-orbit coupling strength.

When spin-orbit coupling is introduced, the symmetry of the metallic ion is described by the D_{4h} double group. The LS state is a representation of A_{1g} , as is the $S^z = 0$ HS state, while the $S^z = \pm 1$ HS states form an E_g irreducible representation. Hence, only the LS state and the $S^z = 0$ HS state are coupled. This results in a $\Delta S^z = 0$ selection rule within the low-energy subspace. Thus, we find that

$$\begin{aligned}
 \hat{H}_{\text{SOC}} &= \xi \sum_{j=1}^N \hat{L}_j^z \hat{S}_j^z, \\
 &= \frac{\xi}{2} \sum_{j=1}^N \sum_{s \in \{\downarrow, \uparrow\}} \sum_{l_m = -2}^2 (-1)^{\delta_{s,\downarrow}} l_m \hat{a}_{j,l_m,s}^\dagger \hat{a}_{j,l_m,s}, \\
 &= i\xi \sum_{j=1}^N \left(\hat{c}_{j,xy,\uparrow}^\dagger \hat{c}_{j,x^2-y^2,\uparrow} - \hat{c}_{j,xy,\downarrow}^\dagger \hat{c}_{j,x^2-y^2,\downarrow} \right. \\
 &\quad \left. + \hat{c}_{j,x^2-y^2,\downarrow}^\dagger \hat{c}_{j,xy,\downarrow} - \hat{c}_{j,x^2-y^2,\uparrow}^\dagger \hat{c}_{j,xy,\uparrow} \right), \\
 &= -i\sqrt{2}\xi \sum_{j=1}^N (|1, 0\rangle_{jj} \langle -1, 0| - |-1, 0\rangle_{jj} \langle 1, 0|).
 \end{aligned} \quad (6)$$

It is convenient to introduce pseudo-spin ladder operators, defined as

$$\begin{aligned}\hat{\sigma}_j^+ |\sigma^z, S^z\rangle_j &= \left(\frac{1 - \sigma^z}{2}\right) |\sigma^z + 2, S^z\rangle_j, \\ \hat{\sigma}_j^- |\sigma^z, S^z\rangle_j &= \left(\frac{1 + \sigma^z}{2}\right) |\sigma^z - 2, S^z\rangle_j.\end{aligned}\quad (7)$$

Whence the spin-orbit coupling can be written as

$$\hat{H}_{\text{SOC}} = \lambda \sum_{j=1}^N \hat{\sigma}_j^y [1 - (\hat{S}_j^z)^2], \quad (8)$$

where $\lambda = \sqrt{2}\xi$, $\hat{\sigma}_j^y = -i(\hat{\sigma}_j^+ - \hat{\sigma}_j^-)$, and the factor $1 - (\hat{S}_j^z)^2 = \delta_{S^z, 0}$ enforces the $\Delta S^z = 0$ selection rule. We only consider the case of $\lambda > 0$ as the spin-orbit coupling constant will be positive for nickel in a square planar geometry [88].

Some insight into the physics engendered by the SOC can be gained by assuming simple orders in one of the spin or pseudo-spin subsystems. If $\langle \hat{S}_j^z \rangle = 0$ for each ion, the SOC acts like a transverse field for the pseudo-spins, similarly to a previously proposed model for SC [74]. Conversely, if $\langle \hat{\sigma}_j^y \rangle = \pm 1$, the SOC acts like a single ion anisotropy for the physical spins.

E. Full model

Finally, we promote the classical pseudo-spin variable in the Wajnflasz–Pick–Ising model to a quantum operator, $\sigma_j^z \rightarrow \hat{\sigma}_j^z$. Summing the three terms described above yields our full model of a magnetically coupled chain of d^8 square planar SC complexes:

$$\begin{aligned}\hat{H} &= \hat{H}_{\text{WPI}} + \hat{H}_X + \hat{H}_{\text{SOC}}, \\ &= J_I \sum_{j=1}^N \hat{\sigma}_j^z \hat{\sigma}_{j+1}^z + \Delta G \sum_{j=1}^N \hat{\sigma}_j^z \\ &\quad + J_H \sum_{j=1}^N \hat{\mathbf{S}}_j \cdot \hat{\mathbf{S}}_{j+1} + \lambda \sum_{j=1}^N \hat{\sigma}_j^y [1 - (\hat{S}_j^z)^2].\end{aligned}\quad (9)$$

An important difference between this model and many other model Hamiltonians for SC systems is that the total spin is not a good quantum number for $\lambda \neq 0$.

III. METHODS

A. Density matrix renormalization group calculations

We solve for the groundstates of Eq. (9) using DMRG [89–91] in the matrix product state (MPS) formalism [92–97] using the ITensor library [98]. We include the LS and three HS states by using a local 4-dimensional Hilbert

space and construct the relevant local operators in the Hamiltonian of the full model [Eq. (9)]. We keep a truncated basis size of the tensors of $m = 700$ for the majority of parameters in the phase diagram, using a smaller or larger m depending on how close the ground state is to a phase boundary. We scale all our results to the $m \rightarrow \infty$ limit using the variance in the internal energy. We study lattice sizes up to $N = 200$ and scale all of our observables to the thermodynamic limit $N \rightarrow \infty$.

B. Order parameters

Several order parameters are required to differentiate the six phases sketched in Fig. 1. For ease of reference we detail them below, before moving on to our results.

1. (Anti)ferroelastic phases

Long-range spin-state order can be identified with local order parameters. The ferroelastic order parameter is analogous to magnetization:

$$m^z = \frac{1}{N} \sum_{j=1}^N \langle \hat{\sigma}_j^z \rangle. \quad (10)$$

$m^z > 0$ ($m^z < 0$) indicates a HS (LS) phase, Fig. 1 a,b,d.

The antiferroelastic order parameter is also analogous to staggered magnetization:

$$m_A^z = \frac{1}{N} \sum_{j=1}^N (-1)^j \langle \hat{\sigma}_j^z \rangle. \quad (11)$$

$m_A^z \neq 0$ indicates long-ranged antiferroelastic order with alternating HS and LS, Fig. 1c.

It will also be helpful to consider a transverse ferroelastic order parameter which measures the ordering described in Fig. 1e,

$$m^y = \frac{1}{N} \sum_{j=1}^N \langle \hat{\sigma}_j^y \rangle. \quad (12)$$

2. Dimer ordering

The dimer phase can be identified by the parameter,

$$\begin{aligned}m^D &= \frac{1}{2N} \sum_{\alpha=1}^3 \sum_{j=1}^N (-1)^{\delta_{\alpha, j\%3}} \langle \hat{\sigma}_j^z \rangle \\ &\quad \times \left(1 - \delta_{\alpha, (j+1)\%3} + (-1)^{\delta_{\alpha, (j+1)\%3}} \langle \hat{\mathbf{S}}_j \cdot \hat{\mathbf{S}}_{j+1} \rangle \right),\end{aligned}\quad (13)$$

where

$$\delta_{\alpha, j\%3} = \frac{1}{3} \left\{ 4 \cos \left[\frac{2\pi}{3} (2j + \alpha - 1) \right] - 1 \right\}. \quad (14)$$

Although this is somewhat mathematically cumbersome the physical interpretation is straightforward: m^D identifies long-range ordered phases with a repeating pattern of one LS complex and then two HS complexes in a spin singlet, as sketched in Fig. 1f.

3. Haldane phase

The Haldane phase is well known from previous work on integer spin Heisenberg models [78, 79]. For odd-integer spins it has SPT order and fractionalized edge states (spin-1/2 for spin-one models) [76, 99]. In contrast to the long-ranged order, an SPT state order cannot be explained by Ginzburg-Landau spontaneous symmetry breaking and cannot be characterized by local order parameters [80–82]. However, the SPT order of the Haldane phase can be protected by any of the following symmetries: dihedral ($D_2 = Z_2 \times Z_2$), time-reversal, or reflection about a bond [76, 80]. Dihedral symmetry leads to the formation of hidden non-local magnetic order [100]. This hidden order can be identified with the non-local trivial,

$$O^i = \lim_{|j-k| \rightarrow \infty} \left\langle \hat{\mathbb{I}}_j \exp(i\pi \sum_{l=j+1}^{k-1} \hat{S}_l^z) \hat{\mathbb{I}}_k \right\rangle, \quad (15)$$

and spin,

$$O^z = - \lim_{|j-k| \rightarrow \infty} \left\langle \hat{S}_j^z \exp(i\pi \sum_{l=j+1}^{k-1} \hat{S}_l^z) \hat{S}_k^z \right\rangle, \quad (16)$$

string order parameters [101], where $\hat{\mathbb{I}}_j$ is the identity operator on site j . If $O^z \neq 0$ and $O^i = 0$ then the state is in the Haldane phase, whereas if $O^z = 0$ and $O^i \neq 0$ there is no hidden string order and the phase is topologically trivial [102].

IV. RESULTS

A. Ferroelastic interactions ($J_I < 0$)

1. Degenerate HS and LS states ($\Delta G = 0$)

For $\Delta G = 0$ and ferroelastic coupling we find three phases: the Haldane high spin (HHS), a topologically trivial high spin (THS) and quantum disordered (QD) phases, Fig. 3.

For weak SOC we find that $O^i = 0$ and $O^z \neq 0$, indicating the Haldane phase. Indeed as $\lambda/J_H \rightarrow 0$ we find $O^z \approx 0.374$, the value found for the pure Heisenberg model [103]. As λ/J_H increases, O^z monotonically decreases to zero until there is a topological quantum phase transition to the THS phase, Fig. 3c.

Throughout the HHS phase there is an extremely large fraction of HS complexes, $m^z \approx 1$, indicating that the

magnetic correlations in the HHS phase are incompatible with dynamic LS impurities. When SOC is strong enough to induce even a very small fraction of LS complexes this rapidly suppresses and destroys the spin string order, and hence the SPT phase. Concomitantly, the large energy cost associated with breaking valence bonds between neighboring HS complexes in the HHS phase protects it against the appearance of LS complexes, stabilizing the phase.

Once the HHS phase is destroyed, increasing λ monotonically increases O^i towards one (Fig. 3c). Simultaneously, $m^z \rightarrow 0$ and $m^y \rightarrow -1$. This occurs because SOC favors a trivial quantum product state with $\hat{S}_i^z = 0$ and $\hat{\sigma}_j^y = -1$ for all sites (see Eq. (8)). Explicitly, for $\lambda \rightarrow \infty$, $O^i \rightarrow 1$ and the ground state is

$$|QD\rangle \equiv \bigotimes_{j=1}^N \frac{1}{\sqrt{2}} (|1, 0\rangle_j - i|-1, 0\rangle_j). \quad (17)$$

In the large λ/J_H limit the $S^z = \pm 1$ HS states are high-energy excitations and become irrelevant. Hence, the model reduces to a transverse field Ising model [83] in this limit. $|QD\rangle$ is precisely the quantum disordered phase expected for this limit.

Physically, the QD state corresponds to a quantum superposition of the LS and $S^z = 0$ HS states at every site. Our model does not include any coupling to the ‘environment’ such as molecular vibrations or lattice phonons, or any external modes. It would be interesting, but beyond the scope of this work, to determine whether such couplings will decohere the superposition, and if so how quickly.

Another interesting question about the QD phase, assuming it remains coherent long enough to be measured, is what signatures it would display. An important probe of the spin-state is metal-ligand bond length, which can be measured via x-ray crystallography. Let us define the metal-ligand bond length operator for the j th complex, \hat{r}_j , which takes the values ${}_j\langle 1, 0 | \hat{r}_j | 1, 0 \rangle_j \equiv r_H$ and ${}_j\langle -1, 0 | \hat{r}_j | -1, 0 \rangle_j \equiv r_L$ when the complex is HS and LS, respectively, and has quantum coherent off-diagonal contributions ${}_j\langle 1, 0 | \hat{r}_j | -1, 0 \rangle_j \equiv r_{\text{coh}} \equiv r'_{\text{coh}} + ir''_{\text{coh}}$. It is important to note that x-ray crystallography measures the average bond length across the sample. A simple calculation yields

$$\frac{1}{N} \sum_{j=1}^N \langle QD | \hat{r}_j | QD \rangle = \frac{r_H + r_L}{2} + r''_{\text{coh}}. \quad (18)$$

As the metal-ligand bond length changes significantly between the LS and HS states of SC complexes we expect r''_{coh} will typically be small. Thus, x-ray crystallography will not distinguish the quantum disordered phase from classical disorder.

A similar analysis will hold for any other measurement that can be written as the sum of local terms. A second measurement common in SC is the magnetic susceptibility, χ , multiplied by temperature, T , given by

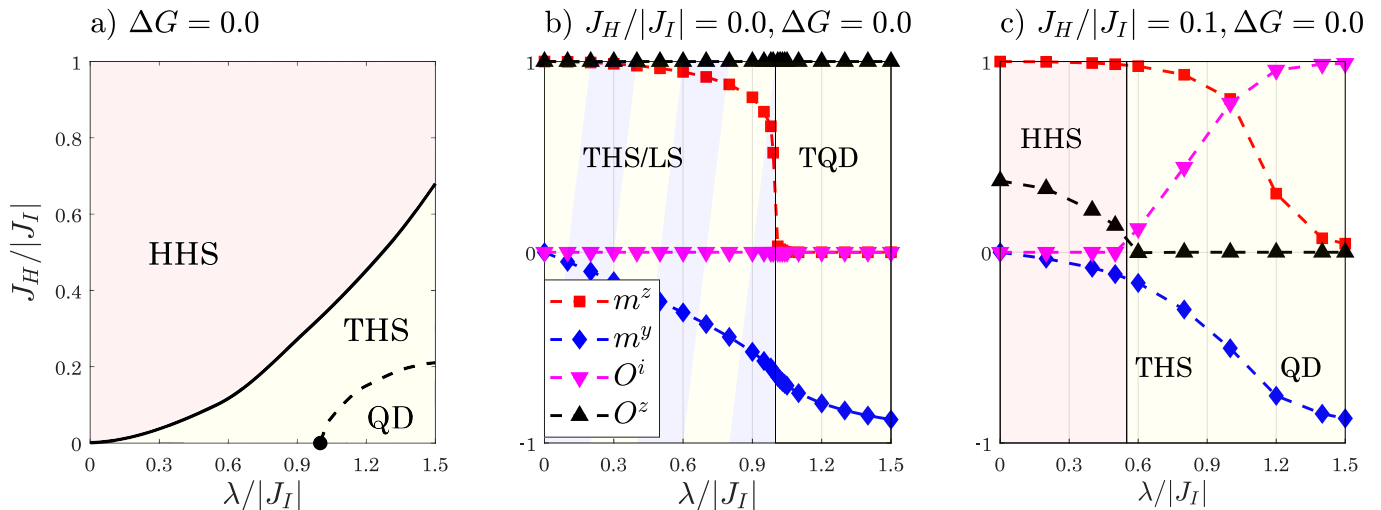


FIG. 3. (a) Phase diagram and (b),(c) order parameters for ferroelastic interactions ($J_I < 0$) and degenerate spin states ($\Delta G = 0$). Spin-orbit coupling (λ) destroys the singlets in the Haldane HS (HHS) phase, leading to a quantum phase transition to a trivial HS (THS) state. Further increasing λ drives a crossover where the spin states become quantum disordered (QD). This phase is adiabatically connected to the large single ion anisotropy (large- D) phase found in spin-one chains. J_H is the antiferromagnetic spin exchange between adjacent sites and $J_I < 0$ is a ferroelastic coupling between sites. In panel (a) the circle denotes a quantum critical point, the phase boundary between the HHS and THS phases is denoted with a solid line, while the dashed line is a guide to the eye marking the crossover from THS to QD. In panels (b,c) m_z (m_y) is the longitudinal (transverse) ferroelastic order parameter defined in Eq. (10) (Eq. (12)) and O^i O^z is the (trivial) string order parameter given by (Eq. (15)) Eq. (16). In the absence of magnetic exchange ($J_H = 0$; panel (b)) the THS and LS phases are degenerate ground states for weak SOC. There is a true quantum phase transition between the THS/LS phase and the QD phase at $\lambda = |J_I|$, which can be understood straightforwardly as corresponding to the quantum phase transition in the transverse field Ising model. Non-zero $\Delta G = 0$ (Section IV A 2) or $J_H = 0$ (panel c) lift the degeneracy between the HS and LS states on individual complexes and drive the quantum phase transition into a crossover.

$\chi^\alpha T = \sum_{j=1}^N \langle S_{N/2}^\alpha S_j^\alpha \rangle$ [104]. As there are no inter-complex magnetic correlations in a product state such as the QD state, χT is a sum of local terms plus a coherent part. However, spin operators (such as S_j^z) do not connect HS and LS states, thus the quantum coherent terms vanish. The expectation of any spin-operator for $|1, 0\rangle_j$ and $|0, 0\rangle_j$ will also be zero, resulting in a vanishing magnetic susceptibility for the ideal QD state [Eq. (17)]. More generally, in the QD phase one should expect some small population of the $|1, \pm 1\rangle_j$ states. These will result in a concomitantly small, but non-zero, χT . In contrast, a classically disordered state of LS and all possible HS states will follow the Curie-Weiss law for a paramagnet, $\chi T \sim (1 - \gamma_{HS}) S_{LS}(S_{LS} + 1) + \gamma_{HS} S_{HS}(S_{HS} + 1) = 2\gamma_{HS}$, where γ_{HS} is the fraction of HS complexes, S_{LS} (S_{HS}) is the spin of the LS (HS) state, and we specialize to square planar d^8 complexes in the final equality.

Thus, the combination of crystallography and magnetic susceptibility measurements is sufficient to identify the QD phase.

At intermediate λ/J_H the many-body physics is more subtle. To understand this regime it is helpful to first consider the model with $J_H = \Delta G = 0$, Fig. 3b. Clearly, with no magnetic interactions between the physical spins the magnetic state is always trivial. We find that $m^y < 0$ and $\langle (S_i^z)^2 \rangle = 0$ for $\lambda > 0$. Thus, we can understand the physics purely from the transverse field Ising model. This

model is well known to have a quantum critical point at $\lambda = |J_I|$, from a ferroelastic spin-state ordered phase (for $\lambda < |J_I|$) to a quantum disordered phase (for $\lambda > |J_I|$) [83]. Unsurprisingly, our numerical results are in good agreement with this, Fig. 3b.

As well as the HHS phase at small λ/J_H , we also find a large region of the phase diagram where $O^z = 0$ and $O^i > 0$ but m^z is large and positive while m^y is small and negative, Fig. 3b. This indicates a topologically trivial HS ferroelastic (THS) phase.

If $\langle \sigma_j^y \rangle$ is small and negative, the SOC (Eq. (8)) acts as a single ion anisotropy for the physical spins, often denoted $D(S^z)^2$. As increasing λ increases $|m^y|$ this generates a super-linear increase in the effective single ion anisotropy. Thus, the HHS to THS phase transition in our model is analogous to the phase transition between the Haldane phase and the large- D phase in the spin-1 Heisenberg model with single ion anisotropy [80].

Single ion anisotropy in a pure spin model arises from SOC, but appears only at second order in λ . In the SC chain we see a related effect, but now occurring at first order in λ . The large- D phase has been widely studied theoretically and the Haldane-to-large- D transition is a canonical example of a topological phase transition in the theoretical literature. There are materials known to realize the Haldane and large- D phases [105], but none offer fine-tuning in order to explore the nature of the phase

transition. Therefore, SC materials, where the equivalent transition is driven by a term at first order in λ , may be an interesting playground to explore this physics experimentally.

The most obvious way to increase SOC is to move to heavier metals. However, this may be problematic here as SC is most commonly observed in complexes of third row transition metals. Nevertheless, this does not mean that SOC cannot be modified [106]. In transition metal complexes the effective spin-orbit coupling is strongly modified by the relativistic nephelauxetic effect [107], which is caused by a combination of: the covalent mixing of the metal and ligand wave functions; the expansion of the d -orbital of the metal in the process of forming a covalent bond with the ligand; and the SOC of the ligand. Thus, ligands with high covalency and large SOC will lead to larger λ .

In our extensive parameter search, we have found that the THS phase always appears as an intermediate phase between the HHS and QD phases for $\Delta G = 0$. SOC suppresses both ferroelastic and spin string order parameters. However, the spin string order is destroyed before the ferroelastic ordering is significantly weakened, Fig. 3b,c. Consequently, to transition from the HHS phase (with $m^z \approx 1$) to the QD phase (with $m^z \rightarrow 0$) the system must pass through the THS phase ($1 > m^z \gg 0$).

There is clear numerical evidence (from the string order parameters, Fig. 3c) that the change from HHS to THS is a continuous (quantum) phase transition. This is consistent with the general expectation on moving from an SPT phase to a topologically trivial phase [80]. For $J_H = 0$ there is a quantum phase transition at $|J_I| \simeq |\lambda|$. However, for $J_H > 0$ we see no evidence of a phase transition between the THS and QD phases numerically, Fig. 3c, and there is no theoretical requirement for a phase transition between them. Therefore, we conclude that the change between these regimes is a crossover. This can be understood because the magnetic interactions lower the energies of neighboring HS complexes, but do not affect LS complexes. Thus, exchange interactions break the Z_2 symmetry of the pseudo-spins, driving the quantum phase transition into a crossover. (Formally, the Z_2 symmetry emerges only once the $S^z = \pm 1$ HS states are projected out of the low-energy model; whence the unitary $\hat{U} \equiv \prod_{j+1}^N \hat{\sigma}_j^y$ maps $\hat{\sigma}_j^z \rightarrow -\hat{\sigma}_j^z$, leaving the Hamiltonian invariant.) This is consistent with the transverse Ising model where a longitudinal field turns the quantum phase transition into a crossover [108, 109].

2. Non-degenerate HS and LS states ($\Delta G \neq 0$)

We do not expect any material to be fine tuned to $\Delta G = 0$ at $T = 0$. For $\Delta G < 0$ (individual HS complexes are lower energy than LS complexes) we find only the three phases present for $\Delta G = 0$. But for sufficiently large $\Delta G > 0$ a ferroelastic LS phase can be induced, Fig. 4. For $\Delta G > 0$ there is a competition between

the single complex physics (ΔG), which favors the LS phase, and antiferromagnetic spin exchange (J_H), which favors spin-singlets that can only occur between HS complexes. Thus, non-zero J_H increases the critical ΔG for the HS-LS phase transition. For $J_H, \Delta G \gg |J_I|, \lambda$ the HS phase is the HHS phase; thus, the HS-LS phase transition moves to $\Delta G \simeq -E_H$, where $E_H \simeq -1.401J_H + \Delta G$ is the energy of the HHS phase. This result is in excellent agreement with our DMRG calculations, even when λ is relatively large, Fig. 4a.

For small λ/J_I the THS phase is pushed to smaller J_H/J_I , Fig. 4a. This emphasises that the introduction of LS impurities, via λ or ΔG , is essential to suppress the HHS phase.

A longitudinal field, $\Delta G \neq 0$, explicitly breaks the Z_2 pseudo-spin symmetry. Consistent with this, our numerics suggests a crossover between THS and QD phases whenever $\Delta G \neq 0$. Again, this follows our expectations from the transverse field Ising model with a longitudinal field [108, 109].

For large $\lambda/|J_I|$, Fig. 4b, we also observe a larger region of THS phase as the HHS is suppressed by the introduction of LS impurities by the SOC.

B. Antiferroelastic interactions ($J_I > 0$)

1. Degenerate HS and LS states ($\Delta G = 0$)

For antiferroelastic coupling we find antiferroelastic (AFE; Fig. 1c) and dimer (Di; Fig. 1f) [59] phases, Fig. 5 along with the HHS, THS, and QD phases. For strong elastic interactions (small J_H/J_I and λ/J_I) we find the AFE phase. Increasing λ drives a phase transition to the QD phase, which is adiabatically connected to the THS phase via a crossover. As J_H/J_I is increased the stability of the AFE phase decreases and the phase boundary to the THS or QD phase is pushed to smaller λ/J_I until the AFE phase disappears at $J_H/J_I \approx 1$.

The antiferromagnetic exchange (J_H) cooperates with ferroelastic interactions ($J_I < 0$) because if there are neighbouring HS states the system can lower its energy by forming spin singlets and developing long-ranged ferroelastic order. In contrast, antiferroelastic interactions ($J_I > 0$) favor alternating HS and LS sites which destroys neighboring HS spin-singlets. The Di phase is a compromise between these two competing interactions. It is found for weak SOC (small λ/J_I) and $J_H \simeq J_I$.

The Di phase balances antiferromagnetic spin exchange and antiferroelastic coupling via long-ranged HS-LS order, with the two adjacent HS forming a spin-singlet, Fig. 1f. Thus, the Di phase is characterized by $m^z \approx 1/3$ and $|m_D| > 0$ (Eq. (13); Fig. 5). This should be evident from crystallography or Mössbauer spectroscopy. However, χT should be small because of both the singlet formation as well as LSs. Thus, combining susceptibility measurements with either crystallography or Mössbauer spectroscopy should provide a distinc-

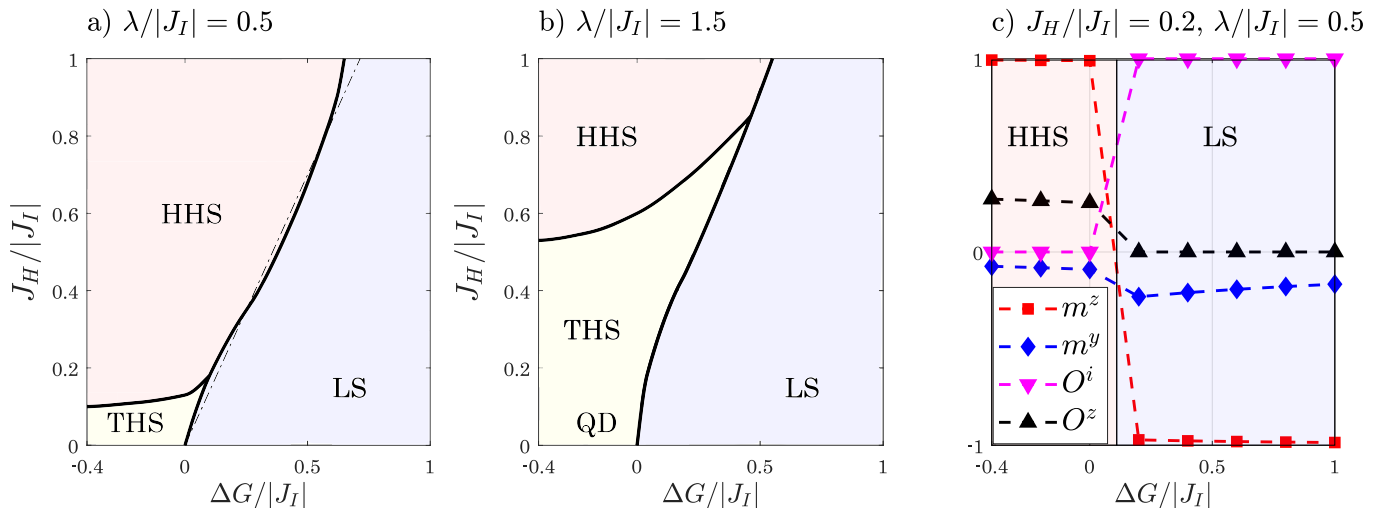


FIG. 4. (a),(b) Phase diagrams and (b) order parameters for ferroelastic interactions with a non-zero Gibbs free energy difference $\Delta G = G_{HS} - G_{LS}$ between individual HS and LS molecules. For both (a) weak ($\lambda = 0.5J_I$) and (b) strong ($\lambda = 1.5J_I$) spin-orbit coupling, increasing ΔG drives a phase transition to a long-ranged LS phase. The dash-dotted line in (a) indicates $\Delta G = E_H$, the simple estimate for the HS-LS phase boundary neglecting λ and J_I , which is in remarkable agreement with the numerical data. The discontinuous change in order parameters as ΔG is varied (c) implies that there is no THS phase between the HHS and LS phases in contrast to the phase diagram for $\Delta G = 0$ (Fig. 3).

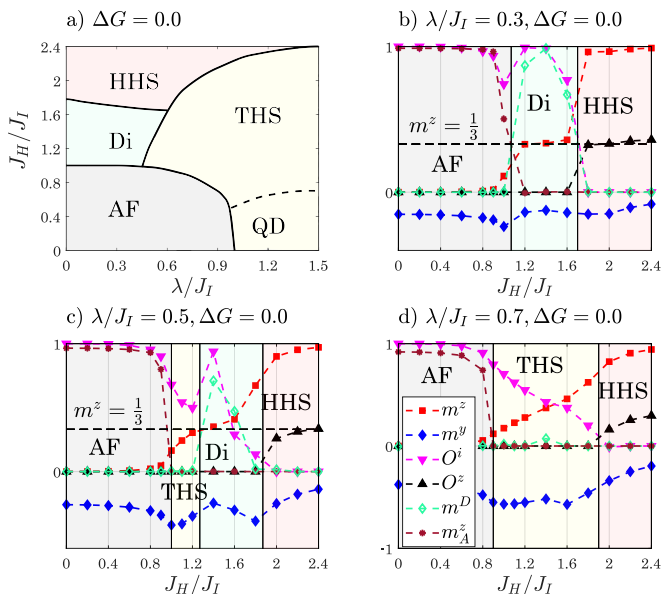


FIG. 5. (a) Phase diagram and (b-d) order parameters for antiferroelastic interactions ($J_I > 0$) and degenerate HS and LS complexes ($\Delta G = 0$). Spin-exchange, which favors spin-singlet formation between HS complexes, competes with the antiferroelastic coupling and SOC; thus the HHS phase is limited to large J_H . For small λ and intermediate J_H there is a compromise and a long-ranged HS-HS-LS dimer (Di; Fig. 1f) order forms with adjacent HS complexes forming spin singlets, indicated by $m^D \neq 0$ (Eq. (13)) and $m^z \simeq 1/3$. For sufficiently large λ , the Di and AFE phases are suppressed due to disorder introduced by dynamical LS impurities.

tive experimental signature of the Di phase.

Alternatively, experiments which measure spin spectral properties of the different phases such as neutron scattering and inelastic electron tunneling spectroscopy (IETS), which is performed with a scanning tunneling microscope, should also be able to identify different SC phases. On a metallic surface, SC molecules in the HS state may show a Kondo resonance, whereas LS molecules will not [41]. This allowed the identification of the AFE phase in NiTHB [41]. Similarly, the Haldane phase has previously been identified using IETS through zero-bias Kondo resonances produced by the fractionalised edge states [110–114]. However, in the dimer phase the HS molecules form valence bonds and so the Kondo resonance zero bias peak should be absent, due to the monogamy of entanglement.

The discontinuous change in the antiferroelastic order parameter (Eq. (11)) suggest that the AFE and Di phases are separated by a first order phase transition, Fig. 5b. For weak SOC and large enough J_H/J_I , spin-singlet formation wins and there is a phase transition to the HHS phase. For $J_H \approx J_I$, increasing SOC drives a phase transition from the Di phase to the THS phase, Fig. 5a,c.

2. Non-degenerate HS and LS states ($\Delta G \neq 0$)

For antiferroelastic interactions large enough $\Delta G > 0$ will drive LS long-ranged ferroelastic ordering ($m^z < 0$), similar to that found for ferroelastic coupling. However, the phase diagram in the antiferroelastic case, Fig. 6, is significantly more complex than the phase diagram for ferroelastic interaction, Fig. 4.

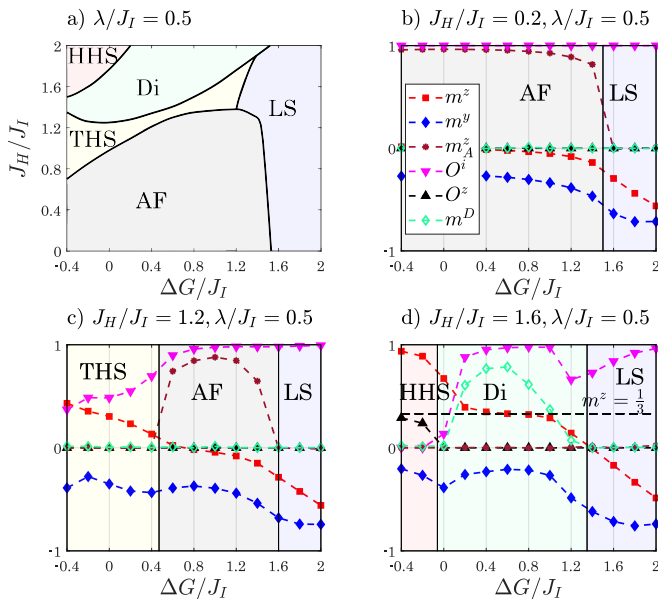


FIG. 6. (a) Phase diagrams and (b-d) order parameters for antiferroelastic interactions ($J_I > 0$) and non-degenerate HS and LS complexes ($\Delta G \neq 0$) for weak SOC ($\lambda = 0.5J_I$). $\Delta G > 0$ stabilizes the AFE and Di phases as it favors LS complexes. For large enough ΔG there is a phase transition to the long-ranged ordered LS phase. Antiferroelastic interactions suppresses both ferroelastic and dimer phases unless ΔG is large.

Notably, for weak SOC, the AFE phase is stable over a wide range of ΔG and weak to intermediate J_H/J_I . This is the phase observed in NiTHB [41]. For larger J_H/J_I , positive ΔG stabilizes the Di phase; although the HHS phase eventually wins out for very strong antiferromagnetic interactions.

There are now phase transitions between the AFE and LS phases, THS and LS phases, and Di and LS phases. However, unlike the ferroelastic case (Fig. 4), we do not find a direct transition between the HHS and LS phases in our numerics, Fig. 6. This indicates that the HHS phase is less resilient to LS impurities when there is antiferroelastic coupling. This is reasonable as we saw that, even for ferroelastic interactions, the HHS phase is rapidly destroyed by the introduction of LS impurities, which antiferroelastic coupling will tend to favor. Once even a small fraction of complexes become LS the Di phase is rapidly favoured as it is able to lower its energy from both antiferroelastic interactions (as two out of every three nearest neighbour are in opposite spin sites) and from antiferromagnetic exchange interactions, Fig. 1f.

However, for strong SOC ($\lambda > J_I$) both the AFE and Di phases are suppressed, Fig. 7, and the phase diagram is now broadly similar to that for ferroelastic interaction, Fig. 4b. Interestingly $\Delta G > 0$ suppresses the QD phase much more strongly than $\Delta G < 0$.

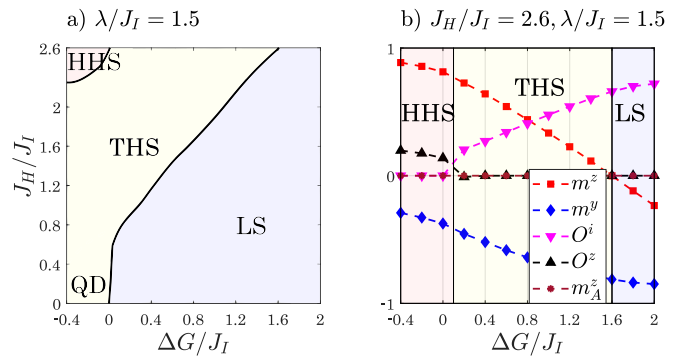


FIG. 7. (a) Phase diagrams and (b) order parameters for antiferroelastic interactions with strong SOC, $\lambda/J_I = 1.5$. Strong SOC suppresses both antiferroelastic and dimer phases and stabilises the QD phase as it promotes quantum disorder in the spin states. Nevertheless, there remains a competition between ΔG which favors long-range LS order and J_H which favors long-range HS order.

V. CONCLUSION

Elastic, magnetic and spin-orbit interactions have all been previously shown to significantly impact the collective behavior of spin crossover materials. We have derived and studied a model of spin crossover materials that treats all of these interactions on an equal footing. We solved the model for a 1D chain of square planar, d^8 complexes using finite DMRG at $T = 0$. This showed a rich phase diagram containing six different phases (Fig. 1) due to the competition between these three different interactions.

SOC is key because it couples the magnetic and spin-state (pseudo-spin) degrees of freedom. For a given (fixed) magnetic state the SOC acts like a transverse field in the Wajnflasz–Pick–Ising model of pseudo-spins. Whereas for a given (fixed) configuration of spin states SOC acts as a single ion anisotropy in the spin-one Heisenberg chain. In the round, SOC couples these two effects (Eq. (8)). The inclusion of SOC allow for dynamic changes of the spin-state of individual complexes, this leads to dynamic impurities and has a profound effect on the collective behaviors.

Because the HS state of square planar d^8 complexes is $S = 1$ the HS phase comes in two forms: an SPT Haldane (HHS) phase and a topologically trivial HS (THS) phase. The Haldane phase is only stable for weak SOC and large antiferromagnetic interactions. This is because the dynamical LS impurities introduced for any sizable SOC rapidly destroy the SPT state and drive the system into the THS phase. For $\lambda > 0$, which we expect physically, SOC favors $S^z = 0$ states, thus the HHS-THS phase transition is equivalent to the Haldane–large-D phase transition driven by single ion anisotropy (D) in the spin-one Heisenberg model.

Sizable SOC ($\lambda \gtrsim |J_I|$), degenerate HS and LS single molecule states ($\Delta G = 0$), and vanishing magnetic inter-

action ($J_H = 0$) implies that the $S^z = \pm 1$ HS states are high-energy excitations and, therefore, do not play a significant role in the low-energy physics. The $S^z = \pm 1$ HS states can therefore be projected out of the low-energy subspace, the resulting model has a Z_2 symmetry corresponding to mapping $\hat{\sigma}_i^z \rightarrow -\hat{\sigma}_i^z$, generated by the unitary $\hat{U} \equiv \prod_{j+1}^N \hat{\sigma}_j^y$. Thus, the system can be understood as a transverse field Ising model with the SOC, λ , playing the role of the transverse field. Consistent with this we find a quantum critical point between the THS and quantum disordered (QD) phases at $\lambda = J_I$ and $\Delta G = J_H = 0$ numerically (without projecting the $S^z = \pm 1$ HS states out of the model). These phases correspond to the ferromagnetic and quantum disordered phases of the transverse field Ising model respectively. However, if either ΔG or J_H are non-zero this lifts the Z_2 symmetry and changes the phase transition into a crossover.

The results above imply that there is adiabatic continuity between the QD phase and the THS phases in our model. More surprisingly, this implies that there is adiabatic continuity between the large-D phase of the spin-one Heisenberg model and the quantum disordered phase of the transverse field Ising model.

For $\Delta G > 0$ we find a ferroelastic LS phase. Naturally, this is more stable for ferroelastic interactions than

antiferroelastic interactions, as the former compete with the single ion physics, whereas the latter cooperate to stabilize the ferroelastic LS phase.

We also find a dimer phase, which results from the competition between antiferromagnetic and antiferroelastic interactions. This is equivalent to the dimer phase previously predicted for chains of d^6 complexes in the absence of SOC by Timm and Schollwöck [59].

Natural questions arising from our work include: What effect do finite temperatures have of the phase diagram, especially do any additional phases occur at finite temperature? What happens in higher dimensional systems? What are the equivalent models for coordination spheres with different symmetries or different fillings of the metallic ions? And how does the emergent physics of such models differ from that described here?

ACKNOWLEDGMENTS

This work was supported by the Australian Research Council (DP230100139), the Australian Government Research Training Program Scholarship, and MEXT Quantum Leap Flagship Program (MEXT Q-LEAP) Grant Number JPMXS0118069605.

-
- [1] N. Montenegro-Pohlhammer, R. S. de Armas, C. J. Calzado, M. Borges-Martínez, and G. Cárdenas-Jirón, A photo-induced spin crossover based molecular switch and spin filter operating at room temperature, *Dalton Trans.* **50**, 6578 (2021).
- [2] P. Gütllich, Y. Garcia, and H. A. Goodwin, Spin crossover phenomena in Fe(II) complexes, *Chem. Soc. Rev.* **29**, 419 (2000).
- [3] J. Cruddas and B. J. Powell, Structure-property relationships and the mechanisms of multistep transitions in spin crossover materials and frameworks, *Inorg. Chem. Front.* **7**, 4424 (2020).
- [4] M. Paez-Espejo, M. Sy, and K. Boukheddaden, Elastic Frustration Causing Two-Step and Multistep Transitions in Spin-Crossover Solids: Emergence of Complex Antiferroelastic Structures, *J. Am. Chem. Soc.* **138**, 3202 (2016).
- [5] N. F. Sciortino, F. Ragon, Y. M. Klein, C. E. Housecroft, C. G. Davies, G. N. L. Jameson, G. Chastanet, and S. M. Neville, Guest-Responsive Elastic Frustration “On–Off” Switching in Flexible, Two-Dimensional Spin Crossover Frameworks, *Inorg. Chem.* **57**, 11068 (2018).
- [6] Y. M. Klein, N. F. Sciortino, F. Ragon, C. E. Housecroft, C. J. Kepert, and S. M. Neville, Spin crossover intermediate plateau stabilization in a flexible 2-D Hofmann-type coordination polymer, *Chem. Commun.* **50**, 3838 (2014).
- [7] F.-L. Liu and J. Tao, Hysteretic Two-Step Spin-Crossover Behavior in Two Two-Dimensional Hofmann-Type Coordination Polymers, *Chem. Eur. J.* **23**, 18252 (2017).
- [8] L. Piñero-López, M. Sereyuk, M. C. Muñoz, and J. A. Real, Two- and one-step cooperative spin transitions in Hofmann-like clathrates with enhanced loading capacity, *Chem. Commun.* **50**, 1833 (2014).
- [9] E. Milin, V. Patinec, S. Triki, E.-E. Bendeif, S. Pillet, M. Marchivie, G. Chastanet, and K. Boukheddaden, Elastic Frustration Triggering Photoinduced Hidden Hysteresis and Multistability in a Two-Dimensional Photoswitchable Hofmann-like Spin-Crossover Metal–Organic Framework, *Inorg. Chem.* **55**, 11652 (2016).
- [10] K. A. Zenere, S. G. Duyker, E. Trzop, E. Collet, B. Chan, P. W. Doheny, C. J. Kepert, and S. M. Neville, Increasing spin crossover cooperativity in 2D Hofmann-type materials with guest molecule removal, *Chem. Sci.* **9**, 5623 (2018).
- [11] M. J. Murphy, K. A. Zenere, F. Ragon, P. D. Southon, C. J. Kepert, and S. M. Neville, Guest Programmable Multistep Spin Crossover in a Porous 2-D Hofmann-Type Material, *J. Am. Chem. Soc.* **139**, 1330 (2017).
- [12] F.-L. Liu, D. Li, L.-J. Su, and J. Tao, Reversible three equal-step spin crossover in an iron(II) Hofmann-type metal–organic framework, *Dalton Trans.* **47**, 1407 (2018).
- [13] N. F. Sciortino, K. R. Scherl-Gruenwald, G. Chastanet, G. J. Halder, K. W. Chapman, J.-F. Létard, and C. J. Kepert, Hysteretic Three-Step Spin Crossover in a Thermo- and Photochromic 3D Pillared Hofmann-type Metal–Organic Framework, *Angew. Chem. Int. Ed.* **51**, 10154 (2012).
- [14] N. F. Sciortino, K. A. Zenere, M. E. Corrigan, G. J. Halder, G. Chastanet, J.-F. Létard, C. J. Kepert, and S. M. Neville, Four-step iron(II) spin state cascade

- driven by antagonistic solid state interactions, *Chem. Sci.* **8**, 701 (2017).
- [15] G. Agustí, M. C. Muñoz, A. B. Gaspar, and J. A. Real, Spin-Crossover Behavior in Cyanide-Bridged Iron(II)–Gold(I) Bimetallic 2D Hofmann-like Metal–Organic Frameworks, *Inorg. Chem.* **47**, 2552 (2008).
- [16] T. Kosone, C. Kachi-Terajima, C. Kanadani, T. Saito, and T. Kitazawa, A Two-step and Hysteretic Spin-crossover Transition in New Cyano-bridged Heterometal Fe(II) Au(I) 2-Dimensional Assemblage, *Chem. Lett.* **37**, 422 (2008).
- [17] G. Agustí, A. B. Gaspar, M. C. Muñoz, P. G. Lacroix, and J. A. Real, Spin Crossover and Paramagnetic Behaviour in Two-Dimensional Iron(II) Coordination Polymers with Stilbazole Push-Pull Ligands*, *Aust. J. Chem.* **62**, 1155 (2009).
- [18] J. E. Clements, J. R. Price, S. M. Neville, and C. J. Kepert, Hysteretic Four-Step Spin Crossover within a Three-Dimensional Porous Hofmann-like Material, *Angew. Chem. Int. Ed.* **55**, 15105 (2016).
- [19] Y. Meng, Q.-Q. Sheng, M. N. Hoque, Y.-C. Chen, S.-G. Wu, J. Tucek, R. Zboril, T. Liu, Z.-P. Ni, and M.-L. Tong, Two-Step Spin-Crossover with Three Inequivalent Fe II sites in a Two-Dimensional Hofmann-Type Coordination Polymer, *Chem. Eur. J.* **23**, 10034 (2017).
- [20] C.-J. Zhang, K.-T. Lian, G.-Z. Huang, S. Bala, Z.-P. Ni, and M.-L. Tong, Hysteretic Four-Step Spin-Crossover in a 3D Hofmann-type Metal–Organic Framework with Aromatic Guest, *Chem. Commun.* **55**, 11033 (2019).
- [21] C.-J. Zhang, K.-T. Lian, S.-G. Wu, Y. Liu, G.-Z. Huang, Z.-P. Ni, and M.-L. Tong, The substituent guest effect on four-step spin-crossover behavior, *Inorg. Chem. Front.* **7**, 911 (2020).
- [22] W. Liu, Y.-Y. Peng, S.-G. Wu, Y.-C. Chen, M. N. Hoque, Z.-P. Ni, X.-M. Chen, and M.-L. Tong, Guest-Switchable Multi-Step Spin Transitions in an Amine-Functionalized Metal–Organic Framework, *Angew. Chem. Int. Ed.* **56**, 14982 (2017).
- [23] G. J. Halder, K. W. Chapman, S. M. Neville, B. Moubaraki, K. S. Murray, J.-F. Létard, and C. J. Kepert, Elucidating the Mechanism of a Two-Step Spin Transition in a Nanoporous Metal–Organic Framework, *J. Am. Chem. Soc.* **130**, 17552 (2008).
- [24] X. Bao, P.-H. Guo, W. Liu, J. Tucek, W.-X. Zhang, J.-D. Leng, X.-M. Chen, I. Gural'skiy, L. Salmon, A. Bousseksou, and M.-L. Tong, Remarkably high-temperature spin transition exhibited by new 2D metal–organic frameworks, *Chem. Sci.* **3**, 1629 (2012).
- [25] C. J. Adams, M. C. Muñoz, R. E. Waddington, and J. A. Real, Cooperative Spin Transition in the Two-Dimensional Coordination Polymer $[\text{Fe}(\text{4,4}'\text{-bipyridine})_2(\text{ncx})_2] \cdot 4\text{H}_2\text{O}$ ($x = \text{s, se}$), *Inorg. Chem.* **50**, 10633 (2011).
- [26] G. J. Halder, C. J. Kepert, B. Moubaraki, K. S. Murray, and J. D. Cashion, Guest-Dependent Spin Crossover in a Nanoporous Molecular Framework Material, *Science* **298**, 1762 (2002).
- [27] D. Chernyshov, M. Hostettler, K. W. Törnroos, and H.-B. Bürgi, Ordering Phenomena and Phase Transitions in a Spin-Crossover Compound—uncovering the Nature of the Intermediate phase of $[\text{Fe}(\text{2-pic})_3]\text{Cl}_2 \cdot \text{EtOH}$, *Angew. Chem. Int. Ed.* **42**, 3825 (2003).
- [28] B. J. C. Vieira, J. T. Coutinho, I. C. Santos, L. C. J. Pereira, J. C. Waerenborgh, and V. da Gama, $[\text{Fe}(\text{nsal2trien})]\text{SCN}$, a New Two-Step Iron(III) Spin Crossover compound, with Symmetry breaking Spin-State Transition and an Intermediate Ordered State, *Inorg. Chem.* **52**, 3845 (2013).
- [29] J.-B. Lin, W. Xue, B.-Y. Wang, J. Tao, W.-X. Zhang, J.-P. Zhang, and X.-M. Chen, Chemical/Physical Pressure Tunable Spin-Transition Temperature and Hysteresis in a Two-Step Spin Crossover Porous Coordination Framework, *Inorg. Chem.* **51**, 9423 (2012).
- [30] A. J. Fitzpatrick, E. Trzop, H. Müller-Bunz, M. M. Dîrtu, Y. Garcia, E. Collet, and G. G. Morgan, Electronic vs. structural ordering in a manganese(III) spin crossover complex, *Chem. Commun.* **51**, 17540 (2015).
- [31] J. Klingele, D. Kaase, M. H. Klingele, J. Lach, and S. Demeshko, Two-step spin crossover in the mononuclear iron(II) complex $[\text{Fe}(\text{L})_2(\text{NCS})_2]$ ($\text{L} = 2,5\text{-di}(2\text{-pyridyl})\text{-1,3,4-thiadiazole}$), *Dalton Trans.* **39**, 1689 (2010).
- [32] K. D. Murnaghan, C. Carbonera, L. Toupet, M. Griffin, M. M. Dîrtu, C. Desplanches, Y. Garcia, E. Collet, J.-F. Létard, and G. G. Morgan, Spin-State Ordering on One Sub-lattice of a Mononuclear Iron(III) Spin Crossover Complex Exhibiting LIESST and TIESST, *Chem. Eur. J.* **20**, 5613 (2014).
- [33] V. Money, C. Carbonera, J. Elhaïk, M. Halcrow, J. Howard, and J.-F. Létard, Interplay Between Kinetically Slow Thermal Spin-Crossover and Metastable High-Spin State Relaxation in an Iron(II) complex with Similar $T_{1/2}$ and T(LIESST), *Chemistry – A European Journal* **13**, 5503 (2007).
- [34] J. Luan, J. Zhou, Z. Liu, B. Zhu, H. Wang, X. Bao, W. Liu, M.-L. Tong, G. Peng, H. Peng, L. Salmon, and A. Bousseksou, Polymorphism-Dependent Spin-crossover: Hysteretic Two-Step Spin Transition with an Ordered [HS–HS–LS] Intermediate Phase, *Inorg. Chem.* **54**, 5145 (2015).
- [35] N. Bréfuel, H. Watanabe, L. Toupet, J. Come, N. Matsumoto, E. Collet, K. Tanaka, and J.-P. Tuchagues, Concerted spin crossover and Symmetry Breaking Yield Three Thermally and One Light-Induced Crystallographic Phases of a Molecular Material, *Angew. Chem. Int. Ed.* **48**, 9304 (2009).
- [36] Z.-Y. Li, H. Ohtsu, T. Kojima, J.-W. Dai, T. Yoshida, B. K. Breedlove, W.-X. Zhang, H. Iguchi, O. Sato, M. Kawano, and M. Yamashita, Direct Observation of Ordered High-Spin–Low-Spin Intermediate States of an Iron(III) Three-Step Spin-Crossover Complex, *Angew. Chem. Int. Ed.* **55**, 5184 (2016).
- [37] R.-J. Wei, Q. Huo, J. Tao, R.-B. Huang, and L.-S. Zheng, Spin-Crossover FeII_4 Squares: Two-Step Complete Spin Transition and Reversible Single-Crystal-to-Single-Crystal Transformation, *Angew. Chem. Int. Ed.* **50**, 8940 (2011).
- [38] T. Matsumoto, G. N. Newton, T. Shiga, S. Hayami, Y. Matsui, H. Okamoto, R. Kumai, Y. Murakami, and H. Oshio, Programmable spin-state switching in a mixed-valence spin-crossover iron grid, *Nat. Commun.* **5**, 3865 (2014).
- [39] M. Nihei, M. Ui, M. Yokota, L. Han, A. Maeda, H. Kishida, H. Okamoto, and H. Oshio, Two-Step Spin Conversion in a Cyanide-Bridged Ferrous Square, *Angew. Chem. Int. Ed.* **44**, 6484 (2005).
- [40] H. Watanabe, K. Tanaka, N. Bréfuel, H. Cailleau, J.-F. Létard, S. Ravy, P. Fertey, M. Nishino, S. Miyashita,

- and E. Collet, Ordering phenomena of high-spin/low-spin states in stepwise spin-crossover materials described by the ANNNI model, *Phys. Rev. B* **93**, 014419 (2016).
- [41] J. Liu, Y. Gao, T. Wang, Q. Xue, M. Hua, Y. Wang, L. Huang, and N. Lin, Collective Spin Manipulation in Antiferroelastic Spin-Crossover Metallo-Supramolecular Chains, *ACS Nano* **14**, 11283 (2020).
- [42] G. Chastanet, C. Desplanches, C. Baldé, P. Rosa, M. Marchivie, and P. Guionneau, A critical review of the T(LIESST) temperature in spin crossover materials – What it is and what it is not, *Chem. Sq.* **2-2**, 1 (2018).
- [43] S. Brooker, Spin crossover with thermal hysteresis: practicalities and lessons learnt, *Chem. Soc. Rev.* **44**, 2880 (2015).
- [44] N. Paradisa, G. Chastanet, T. Palamarciuc, P. Rosa, F. Varret, K. Boukheddaden, and J.-F. Létard, Detailed Investigation of the Interplay Between the Thermal Decay of the Low Temperature Metastable HS State and the Thermal Hysteresis of Spin-Crossover Solids, *J. Phys. Chem. C* **119**, 1932 (2011).
- [45] M. Nadeem, J. Cruddas, G. Ruzzi, and B. J. Powell, Toward High-Temperature Light-Induced Spin-State Trapping in Spin-Crossover Materials: The Interplay of Collective and Molecular Effects, *J. Am. Chem. Soc.* **144**, 9138 (2022).
- [46] A. Hauser, Intersystem crossing in Fe(II) coordination compounds, *Coor. Chem. Rev.* **111**, 275 (1991).
- [47] A. Hauser, J. Jeftić, H. Romstedt, R. Hinek, and H. Spiering, Cooperative phenomena and light-induced bistability in iron(II) spin-crossover compounds, *Coor. Chem. Rev.* **190-192**, 471 (1999).
- [48] M. Buron-Le Cointe, N. Ould Moussa, E. Trzop, A. Moréac, G. Molnar, L. Toupet, A. Bousseksou, J. F. Létard, and G. S. Matouzenko, Symmetry breaking and light-induced spin-state trapping in a mononuclear Fe^{II} complex with the two-step thermal conversion, *Phys. Rev. B* **82**, 214106 (2010).
- [49] C. Enachescu, J. Linares, F. Varret, K. Boukheddaden, E. Codjovi, S. G. Salunke, and R. Mukherjee, Nonexponential relaxation of the metastable state of the spin-crossover system [Fe(L)₂(ClO₄)₂·H₂O [L = 2,6-Bis(pyrazole-1-ylmethyl)pyridine], *Inor. Chem.* **43**, 4880 (2004).
- [50] V. Mishra, R. Mukherjee, J. Linares, C. Balde, C. Desplanches, J.-F. Létard, E. Collet, L. Toupet, M. Castro, and F. Varret, Temperature-Dependent Interactions and Disorder in the Spin-Transition Compound [FeII(L)₂](ClO₄)₂·C₇H₈ Through Structural, Calorimetric, Magnetic, Photomagnetic, and Diffuse Reflectance Investigations, *Inor. Chem.* **47**, 7577 (2008).
- [51] G. Chastanet, N. F. Sciortino, S. M. Neville, and C. J. Kepert, High Spin to Low Spin Relaxation Regime Change in a Multistep 3D Spin-Crossover Material, *Eur. J. Inorg. Chem.* **2018**, 314 (2018).
- [52] L. J. Kershaw Cook, H. J. Shepherd, T. P. Comyn, C. Baldé, O. Cespedes, G. Chastanet, and M. A. Halcrow, Decoupled Spin Crossover and Structural Phase Transition in a Molecular Iron (II) complex, *Chem. Eur. J.* **21**, 4805 (2015).
- [53] V. A. Money, C. Carbonera, J. Elhaik, M. A. Halcrow, J. A. Howard, and J.-F. Létard, Interplay between kinetically slow thermal spin-crossover and metastable high-spin state relaxation in an iron(II) complex with similar $T_{1/2}$ and $T_{(LIESST)}$, *Chem. Eur. J.* **13**, 5503 (2007).
- [54] C. Enachescu, J. Linares, E. Codjovi, K. Boukheddaden, and F. Varret, Non-linear behaviour of the spin transition compounds during photo-excitation and relaxation, *J. Optoelectron. Adv. M.* **5**, 261 (2003).
- [55] C. Baldé, W. Bauer, E. Kaps, S. Neville, C. Desplanches, G. Chastanet, B. Weber, and J. F. Létard, Light-Induced Excited Spin-State Properties in 1D Iron(II) Chain Compounds, *Eur. J. Inorg. Chem.* **2013**, 2744 (2013).
- [56] J. A. Rodríguez-Velamazán, C. Carbonera, M. Castro, E. Palacios, T. Kitazawa, J.-F. Létard, and R. Burrell, Two-step thermal spin transition and LIESST relaxation of the polymeric spin-crossover compounds Fe(X-py)₂[Ag(CN)₂]₂ (x=h, 3-methyl, 4-methyl, 3,4-dimethyl, 3-cl), *Chem. Eur. J.* **16**, 8785 (2010).
- [57] G. Chastanet, N. F. Sciortino, S. M. Neville, and C. J. Kepert, High spin to Low Spin Relaxation Regime Change in a Multistep 3D Spin-Crossover Material, *Eur. J. Inorg. Chem.* **2018**, 314 (2018).
- [58] E. Trzop, D. Zhang, L. Piñero-Lopez, F. J. Valverde-Muñoz, M. Carmen Muñoz, L. Palatinus, L. Guerin, H. Cailleau, J. Real, and E. Collet, First Step Towards a Devil's Staircase in Spin-Crossover Materials, *Angew. Chem. Int. Ed.* **55**, 8675 (2016).
- [59] C. Timm and U. Schollwöck, Ground-state phases in spin-crossover chains, *Phys. Rev. B* **71**, 224414 (2005).
- [60] J. Cruddas, G. Ruzzi, and B. J. Powell, Spin-state smectics in spin crossover materials, *J. Appl. Phys.* **129**, 185102 (2021).
- [61] J. Cruddas and B. J. Powell, Spin-State Ice in Elastically Frustrated Spin-Crossover Materials, *J. Am. Chem. Soc.* **141**, 19790 (2019).
- [62] J. Cruddas and B. J. Powell, Multiple Coulomb phases with temperature-tunable ice rules in pyrochlore spin-crossover materials, *Phys. Rev. B* **104**, 024433 (2021).
- [63] J. Cruddas and B. J. Powell, Structure–property relationships and the mechanisms of multistep transitions in spin crossover materials and frameworks, *Inorg. Chem. Front.* **7**, 4424 (2020).
- [64] M. Nishino, Y. Singh, K. Boukheddaden, and S. Miyashita, Tutorial on elastic interaction models for multistep spin-crossover transitions, *J. Appl. Phys.* **130**, 141102 (2021).
- [65] A. I. Popa, L. Stoleriu, and C. Enachescu, Tutorial on the elastic theory of spin crossover materials, *J. Appl. Phys.* **129**, 131101 (2021).
- [66] M. Ndiaye, Y. Singh, H. Fourati, M. Sy, B. Lo, and K. Boukheddaden, Isomorphism between the electroelastic modeling of the spin transition and Ising-like model with competing interactions: Elastic generation of self-organized spin states, *J. Appl. Phys.* **129**, 153901 (2021).
- [67] J. Wajnfłasz and R. Pick, Transition low spin high spin dans les complexes de Fe²⁺, *Le J. Phys. Colloq.* **32**, C1 (1971).
- [68] C. Timm and C. J. Pye, Reentrant magnetic ordering and percolation in a spin-crossover system, *Phys. Rev. B* **77**, 214437 (2008).
- [69] C. Timm, Collective effects in spin-crossover chains with exchange interaction, *Phys. Rev. B* **73**, 014423 (2006).
- [70] K. Boukheddaden, J. Linares, R. Tanasa, and C. Chong, Theoretical investigations on an axial next nearest neighbour Ising-like model for spin crossover solids:

- One- and two-step spin transitions, *J. Phys. Condens. Matter* **19**, 106201 (2007).
- [71] M. Nadeem and B. Powell, Theory of the Relaxation of Trapped Spin-States in spin crossover Materials: Drosophila for Complex Dynamics, ChemRxiv doi:10.26434/chemrxiv-2023-xrj86 (2023).
- [72] H. O. Jeschke, L. Andrea Salguero, B. Rahaman, C. Buchsbaum, V. Pashchenko, M. U. Schmidt, T. Saha-Dasgupta, and R. Valentí, Microscopic modeling of a spin crossover transition, *New J. Phys.* **9**, 448 (2007).
- [73] E. Buhks, G. Navon, M. Bixon, and J. Jortner, Spin conversion processes in solutions, *J. Am. Chem. Soc.* **102**, 2918 (1980).
- [74] G. D'Avino, A. Painelli, and K. Boukheddaden, Vibronic model for spin crossover complexes, *Phys. Rev. B* **84**, 104119 (2011).
- [75] M. Nishino, K. Boukheddaden, S. Miyashita, and F. Varret, Dynamical aspects of photoinduced magnetism and spin-crossover phenomena in Prussian blue analogs, *Phys. Rev. B* **72**, 064452 (2005).
- [76] F. Pollmann, E. Berg, A. M. Turner, and M. Oshikawa, Symmetry protection of topological phases in one-dimensional quantum spin systems, *Phys. Rev. B* **85**, 075125 (2012).
- [77] J. Liu, J. Li, Q. Chen, Q. Xue, Y. Wang, B. Di, Y. Wang, and K. Wu, Lattice-Directed Stabilization of Different Spin-State Phases in Metallo-Supramolecular Chains on Au Surfaces, *Chem. Mater.* **33**, 6166 (2021).
- [78] F. Haldane, Continuum dynamics of the 1-D Heisenberg antiferromagnet: Identification with the O(3) nonlinear sigma model, *Phys. Lett. A* **93**, 464 (1983).
- [79] F. D. M. Haldane, Nonlinear Field Theory of Large-Spin Heisenberg Antiferromagnets: Semiclassically Quantized Solitons of the One-Dimensional Easy-Axis Néel State, *Phys. Rev. Lett.* **50**, 1153 (1983).
- [80] Z.-C. Gu and X.-G. Wen, Tensor-entanglement-filtering renormalization approach and symmetry-protected topological order, *Phys. Rev. B* **80**, 155131 (2009).
- [81] T. Senthil, Symmetry-Protected Topological Phases of Quantum Matter, *Annu. Rev. Condens. Matter Phys.* **6**, 299 (2015).
- [82] X.-G. Wen, Colloquium: Zoo of quantum-topological phases of matter, *Rev. Mod. Phys.* **89**, 041004 (2017).
- [83] S. Sachdev, Introduction, in *Quantum Phase Transitions* (Cambridge University Press, 2011) p. 3–17, 2nd ed.
- [84] S. Sugano, Y. Tanabe, and H. Kamimura, in *Multiplets of Transition-Metal Ions in Crystals* (Academic Press, 1970) 1st ed.
- [85] C. J. Ballhausen, *Introduction to ligand field theory* (McGraw-Hill, 1962) pp. 57–69.
- [86] J. Kanamori, Superexchange interaction and symmetry properties of electron orbitals, *J. Phys. Chem. Solids* **10**, 87 (1959).
- [87] Y. Garcia, P. J. van Koningsbruggen, G. Bravic, P. Guionneau, D. Chasseau, G. L. Cascarano, P. Moscovici, K. Lambert, A. Michalowicz, O. Kahn, and et al., Synthesis, Crystal Structure, EXAFS, and Magnetic Properties of catena-Poly[μ -tris(4-(2-hydroxyethyl)-1,2,4-triazole-*n*1,*n*2)copper(II)] Diperchlorate Trihydrate: Relevance with the Structure of the Iron(II) 1,2,4-Triazole Spin Transition Molecular Materials, *Inorg. Chem.* **36**, 6357 (1997).
- [88] M. Georgiev and H. Chamati, Fine Structure and the Huge Zero-Field Splitting in Ni²⁺ Complexes, *Mol.* **27**, 8887 (2022).
- [89] S. R. White, Density matrix formulation for quantum renormalization groups, *Phys. Rev. Lett.* **69**, 2863 (1992).
- [90] S. R. White, Density-matrix algorithms for quantum renormalization groups, *Phys. Rev. B* **48**, 10345 (1993).
- [91] U. Schollwöck, The density-matrix renormalization group, *Rev. Mod. Phys.* **77**, 259 (2005).
- [92] S. Rommer and S. Östlund, Class of ansatz wave functions for one-dimensional spin systems and their relation to the density matrix renormalization group, *Phys. Rev. B* **55**, 2164 (1997).
- [93] J. Dukelsky, M. A. Martín-Delgado, T. Nishino, and G. Sierra, Equivalence of the variational matrix product method and the density matrix renormalization group applied to spin chains, *EPL* **43**, 457 (1998).
- [94] I. P. McCulloch, From density-matrix renormalization group to matrix product states, *J. Stat. Mech.: Theory Exp.* **2007** (10), P10014.
- [95] N. Schuch, M. M. Wolf, F. Verstraete, and J. I. Cirac, Entropy scaling and simulability by matrix product states, *Phys. Rev. Lett.* **100**, 030504 (2008).
- [96] I. V. Oseledets, Tensor-Train Decomposition, *SIAM J. Sci. Comput.* **33**, 2295 (2011).
- [97] U. Schollwöck, The density-matrix renormalization group in the age of matrix product states, *Ann. Phys.* **326**, 96 (2011).
- [98] M. Fishman, S. R. White, and E. M. Stoudenmire, The ITensor Software Library for Tensor Network Calculations, *SciPost Phys. Codebases*, 4 (2022).
- [99] I. Affleck, T. Kennedy, E. H. Lieb, and H. Tasaki, Valence bond ground states in isotropic quantum antiferromagnets, *Commun. Math. Phys.* **115**, 477 (1988).
- [100] T. Kennedy and H. Tasaki, Hidden symmetry breaking and the Haldane phase in S=1 quantum spin chains, *Commun. Math. Phys.* **147**, 431 (1992).
- [101] M. den Nijs and K. Rommelse, Preroughening transitions in crystal surfaces and valence-bond phases in quantum spin chains, *Phys. Rev. B* **40**, 4709 (1989).
- [102] F. Pollmann and A. M. Turner, Detection of symmetry-protected topological phases in one dimension, *Phys. Rev. B* **86**, 125441 (2012).
- [103] S. R. White and D. A. Huse, Numerical renormalization-group study of low-lying eigenstates of the antiferromagnetic S=1 Heisenberg chain, *Phys. Rev. B* **48**, 3844 (1993).
- [104] A. E. Feiguin and S. R. White, Finite-temperature density matrix renormalization using an enlarged Hilbert space, *Phys. Rev. B* **72**, 220401 (2005).
- [105] O. V. Maximova, S. V. Streltsov, and A. N. Vasiliev, Long range ordered, dimerized, large-D and Haldane phases in spin 1 chain compounds, *Crit. Rev. Solid State Mater. Sci.* **46**, 371 (2021).
- [106] M. Nadeem, J. Cruddas, G. Ruzzi, and B. J. Powell, Toward high-temperature light-induced spin-state trapping in spin-crossover materials: the interplay of collective and molecular effects, *J. Am. Chem. Soc.* **144**, 9138 (2022).
- [107] F. Neese and E. I. Solomon, Calculation of zero-field splittings, g-values, and the relativistic nephelauxetic effect in transition metal complexes. application to high-spin ferric complexes, *Inorganic Chemistry* **37**, 6568

- (1998).
- [108] K. Uzelac, R. Jullien, and P. Pfeuty, One-dimensional transverse-field Ising model in a complex longitudinal field from a real-space renormalization-group method at $T=0$, *Phys. Rev. B* **22**, 436 (1980).
- [109] C. J. Turner, K. Meichanetzidis, Z. Papić, and J. K. Pachos, Optimal free descriptions of many-body theories, *Nat. Comm.* **8**, 2041 (2017).
- [110] C. F. Hirjibehedin, C. P. Lutz, and A. J. Heinrich, Spin Coupling in Engineered Atomic Structures, *Science* **312**, 1021 (2006).
- [111] J. Fransson, O. Eriksson, and A. V. Balatsky, Theory of spin-polarized scanning tunneling microscopy applied to local spins, *Phys. Rev. B* **81**, 115454 (2010).
- [112] J. Fernández-Rossier, Theory of Single-Spin Inelastic Tunneling Spectroscopy, *Phys. Rev. Lett.* **102** (2009).
- [113] F. Delgado, C. D. Batista, and J. Fernández-Rossier, Local Probe of Fractional Edge States of $S = 1$ Heisenberg Spin Chains, *Phys. Rev. Lett.* **111**, 167201 (2013).
- [114] S. Mishra, G. Catarina, F. Wu, R. Ortiz, D. Jacob, K. Eimre, J. Ma, C. A. Pignedoli, X. Feng, P. Ruffieux, J. Fernández-Rossier, and R. Fasel, Observation of fractional edge excitations in nanographene spin chains, *Nat.* **598**, 287 (2021).